PCCP

Supporting Information for:

Detecting Weak Signals from Interfaces by High Accuracy Phase-Resolved SFG Spectroscopy

Martin Thämer,*[a] R. Kramer Campen,[a] and Martin Wolf[a]

This document provides supplementary information to "Detecting Weak Signals from Interfaces by High Accuracy Phase-Resolved SFG Spectroscopy". It includes more details about the experimental setup and the simulation of the signal to noise which is shown in the main text. Additionally, the calibration procedures for the simultaneous referencing and the movement of the traslation stage are shown.

1 Generation of Input Laser Pulses

The different input beams for the spectrometer are generated with 2.2 mJ of 800 nm pulses from an amplified Ti:sapphire laser system (Legend Elite duo with Vitesse Oscillator, total pulse energy 8 mJ, pulse length 50 fs and a repetition rate of 1 kHz). The 2.2 mJ are split into two portions, 2 mJ for the generation of infrared light and 200 μJ which are used as 800 nm upconversion beam. The 2 mJ output is used to pump a commercial OPA with DFG stage (TOPAS, Light Conversion) yielding tunable infrared light (3-10 μm) with pulse energies of ca. 10 μJ (at 3 μm). To pre-compensate for group velocity dispersion (GVD) introduced in the infrared pulses by transmission through the germanium based incoupling optics inside the interferometer (see experimental section in the main text) a specific amount of CaF_2 (negative GVD) is inserted in the infrared beam path.[1]. Using this technique, the infrared pulses could successfully be compressed to pulses durations below 70 fs. The resulting infrared beam is guided into the interferometer. The second portion (200 μJ) of 800 nm light passes through a waveplate and is reflected off a prism surface which is mounted at Brewster's angle. This combination acts as variable attenuator for the 800 nm beam giving tunable pulse energies from 0 - 50 μJ. The 800 nm beam is then sent to a delay line equipped with a computer controlled translation stage (Newport, GTS 150) where the timing between the infrared and 800 nm pulses can be controlled. A subsequent combination of a waveplate and a polarizer allows for tuning the polarization of the visible upconversion beam before it is sent into the interferometer.

2 Data Acquisition and Data Treatment

To acquire the full interferogram (sample and reference), the miniature translation stage is scanned (step scanning) through the desired time delays while 500 laser shots are recorded at each position. In each set of these 500 laser shots 250 belong to the sample- and reference response, respectively. A TTL signal from the electrical driver of the galvanic mirror is recorded simultaneously to the detector responses allowing for automated assignment of each shot into sample and reference signal. This way 4 data columns are generated (detector A sample, detector B sample, detector A reference, and detector B reference) each with 250 entries. Subsequently, the 250 values in each column are averaged and the quotient of the difference and the sum of detector A and detector B is calculated yielding one data point in each of the 2 interferograms (sample and reference). This procedure is then repeated for all stage positions to obtain the full interferograms. The latter (sample and reference interferogram) are in the following windowed (Hanning window) and zero-padded to twice the length before being Fourier-transformed into the frequency domain.

3 Simulation of the Signal to Noise Ratio

The measured intensity of the heterodyned SFG signal in the presented spectrometer I_{het} can be expressed in the time domain by following equation

$$I_{het}(t_{IR}) = \beta \cdot \int_{-\infty}^{\infty} dt (E_{LO}(t+t_{IR}) + E_{SFG}(t,t_{IR}))^2 \qquad (1)$$

with the fields of the local oscillator (LO) and the SFG signal E_{LO} and E_{SFG}, respectively. β is a constant and t_{IR} represents the time delay between the infrared and the combined LO and upconversion pulses. In a first step we normalize the fields of the LO and the SFG signal by the square root of their signal intensity. In contrast to the LO the intensity of the SFG signal varies with t_{IR}. We therefore use for its normalization the maximum intensity.

$$E_{SFG}(t,t_{IR}) = \sqrt{\frac{1}{\beta} I_{SFG}^{\max}} \cdot \|E_{SFG}(t,t_{IR})\| \qquad (2)$$

[a] Fritz Haber Institute of the Max Planck Society, 4-6 Faradayweg, 14195 Berlin, Germany

$$E_{LO}(t+t_{IR}) = \sqrt{\frac{1}{\beta} I_{LO}} \cdot \|E_{LO}(t+t_{IR})\| \tag{3}$$

By noting that

$$\int_{-\infty}^{\infty} dt(\|E_{LO}(t+t_{IR})\|)^2 = 1 \tag{4}$$

and by defining the new time delay dependent functions $\mathscr{A}(t_{IR})$ and $\mathscr{J}(t_{IR})$

$$\int_{-\infty}^{\infty} dt(\|E_{SFG}(t,t_{IR})\|)^2 = \mathscr{A}(t_{IR}) \tag{5}$$

$$\int_{-\infty}^{\infty} dt\,(\|E_{SFG}(t,t_{IR})\| \cdot \|E_{LO}(t+t_{IR})\|) = \mathscr{J}(t_{IR}) \tag{6}$$

equation 1 can be transformed into

$$I_{het}(t_{IR}) = I_{LO} + I_{SFG}^{\max} \cdot \mathscr{A}(t_{IR}) + 2\sqrt{I_{LO} I_{SFG}^{\max}} \cdot \mathscr{J}(t_{IR}) \tag{7}$$

The function $\mathscr{A}(t_{IR})$ smoothly varies between 0 and 1 and describes the normalized time delay dependent SFG signal intensity whereas $\mathscr{J}(t_{IR})$ represents the normalized interferogram. For the theoretical description of the signal to noise ratio we assume the presence of four dominant noise sources. Most prominent is noise from intensity fluctuations of the laser pulses. In both SFG components the SFG signal and the local oscillator this intensity noise is present and because they are generated with the same pair of infrared and 800 nm pulses their fluctuations are strongly correlated. Their intensities for each single laser shot show therefore approximately the same relative deviation Δ_{int} from the corresponding mean intensities as expressed in equations 8 and 9.

$$I_{LO} = \overline{I_{LO}}\,(1+\Delta_{\text{int}}) \tag{8}$$

$$I_{SFG}^{\max} = \overline{I_{SFG}^{\max}} \cdot (1+\Delta_{\text{int}}) \tag{9}$$

Additional noise originates from the detection process and can be divided into shot noise (Δ_{shot}), background noise (Δ_{b}), and pulse intensity dependent amplification noise (Δ_{amp}). The amplitude of the shot noise scales with the square root of the light intensity that enters the detector, whereas the background noise is independent of the light intensities. The amplification noise meanwhile originates from fluctuations of the amplification gain and scales linearly with the detected light intensity. Combining all three detection related noise sources which are represented by the (relative) deviations Δ_{i} from the mean values the measured intensity I_{det} can be described by following equation.

$$I_{\text{det}} = \left(I_{het}(t_{IR}) + \sqrt{I_{het}(t_{IR})} \cdot \Delta_{shot}\right) \cdot \left(1+\Delta_{amp}\right) + \Delta_b \tag{10}$$

Combining equations 7 to 10 finally yields the full expression for the case of simple heterodyning.

$$I_{\text{det}}(t_{IR}) = \left(\overline{I_{het}(t_{IR})} \cdot (1+\Delta_{\text{int}}) + \sqrt{\overline{I_{het}(t_{IR})} \cdot (1+\Delta_{\text{int}})} \cdot \Delta_{shot}\right) \cdot \left(1+\Delta_{amp}\right) + \Delta_b \tag{11}$$

Using the balanced detection scheme described in the main text two output beams are generated where the fields of the SFG signal and the LO are combined with opposite signs. The corresponding light intensities $I^{(1)}$ and $I^{(2)}$ are given by 12 and 13.

$$I^{(1)}{}_{het}(t_{IR}) = \beta \frac{1}{2} \int_{-\infty}^{\infty} dt(E_{LO}(t+t_{IR}) + E_{SFG}(t,t_{IR}))^2 \tag{12}$$

$$I^{(2)}{}_{het}(t_{IR}) = \beta \frac{1}{2} \int_{-\infty}^{\infty} dt(E_{LO}(t+t_{IR}) - E_{SFG}(t,t_{IR}))^2 \tag{13}$$

Applying the same normalization as shown above and including the four noise sources yields for the detected signals following expressions.

$$I_{\text{det}}^{(1)}(t_{IR}) = \left(\frac{1}{2}\overline{I_{het}^{(1)}(t_{IR})} \cdot (1+\Delta_{\text{int}}) + \sqrt{\frac{1}{2}\overline{I_{het}^{(1)}(t_{IR})} \cdot (1+\Delta_{\text{int}})} \cdot \Delta_{shot}^{(1)}\right) \cdot \left(1+\Delta_{amp}^{(1)}\right) + \Delta_b^{(1)} \tag{14}$$

$$I_{\text{det}}^{(2)}(t_{IR}) = \left(\frac{1}{2}\overline{I_{het}^{(2)}(t_{IR})} \cdot (1+\Delta_{\text{int}}) + \sqrt{\frac{1}{2}\overline{I_{het}^{(2)}(t_{IR})} \cdot (1+\Delta_{\text{int}})} \cdot \Delta_{shot}^{(2)}\right) \cdot \left(1+\Delta_{amp}^{(2)}\right) + \Delta_b^{(2)} \tag{15}$$

Since the two detection channels are completely independent they produce uncorrelated amplification, shot, and background noise (indicated by the different indices). The sum and the differences of the measured intensities can then be formed based on equations 14 and 15. For the reduction of the contribution of the intensity noise (INS technique, see main text) we finally form the quotient Q_{det} between the difference and the sum of the detected signals.

$$Q_{\text{det}}(t_{IR}) = \frac{\Delta I_{\text{det}}(t_{IR})}{\Sigma I_{\text{det}}(t_{IR})} \tag{16}$$

The simulation of the S/N ratio is based on the equations derived above. Three different cases are hereby analyzed, the case of simple heterodyning using the full SFG signal and LO intensities (equation 11), heterodyning with balanced detection and taking the difference of the detector outputs (14-15), and finally heterodyning with balanced detection and taking the quotient between the difference and the sum of the detector outputs (equation 16). For the simulation independent Gaussian noise traces $g^{(\text{i})}(\sigma^{(\text{i})})$ with 100,000 data points are generated for each independent noise source (i) with the corresponding standard deviations $\sigma^{(\text{i})}$. These traces are subsequently inserted into equations 11, 14, 15 and 16 replacing the Δ_{i}. The resulting noisy intensity traces represent the outcome of the corresponding experiment. From here the signal to noise ratios can be computed by dividing the signal amplitude by the standard deviation of the data points within the intensity trace. As signal amplitude we use the amplitude of the interference term because this is the contribution that carries the spectroscopic information. It can easily be extracted for each of the three cases from the corresponding equation (with the noise contributions set to zero).

In the example simulation shown in figure 3A (main text) we used the following noise contributions representing typical values for heterodyned SFG experiments. The relative intensity noise and the amplification noise are set to 6% and 1%, respectively. The background noise amounts to 25% of the sample SFG intensity (I_{SFG}) and for the shot noise we assumed a noise contribution of 5% with respect to I_{SFG}. Latter value corresponds to the case where roughly 400 SFG photons are generated at the sample surface.

4 Determination of Noise Parameter of the Spectrometer

The magnitude of the different noise contributions is determined experimentally by selectively blocking different beam components and recording a set of 10,000 subsequent laser shots. For the LO intensities used in the experiment the noise contributions follow a clear hierarchy expressed by equation 17 which highly simplifies their determination.

$$\overline{I_{LO}}\,(1+\Delta_{\mathrm{int}}) \gg \overline{I_{LO}}\left(1+\Delta_{amp}\right) \gg \Delta_b \tag{17}$$

Blocking the entire infrared beam eliminates the LO beam and the SFG signal from the sample. Each detector output then obviously shows the correspondent background noise (equation 18).

$$I^{(1)}_{\mathrm{det}}(t_{IR}) = \Delta^{(1)}_b \;;\; I^{(2)}_{\mathrm{det}}(t_{IR}) = \Delta^{(2)}_b \tag{18}$$

The standard deviation of the n acquired data points $\sigma(I_{\mathrm{det}}(t_{IR}),n)$ from both traces equals the standard deviations of the background noise σ_b.

$$\sigma^{(1)}_b = \sigma(I^{(1)}_{\mathrm{det}}(t_{IR}),n) \;;\; \sigma^{(2)}_b = \sigma(I^{(2)}_{\mathrm{det}}(t_{IR}),n) \tag{19}$$

In a subsequent experiment only the infrared portion for the SFG signal from the sample is blocked. Using the relation 14 and 15 the measured difference of the detector outputs is given by following equation.

$$\Delta I_{\mathrm{det}}(t_{IR}) = \frac{1}{2}\overline{I_{LO}}\,(1+\Delta_{\mathrm{int}})\cdot\left(\Delta^{(1)}_{amp}-\Delta^{(2)}_{amp}\right)+$$
$$\sqrt{\frac{1}{2}\overline{I_{LO}}\cdot(1+\Delta_{\mathrm{int}})}\cdot\left(\Delta^{(1)}_{shot}\left(1+\Delta^{(1)}_{amp}\right)-\Delta^{(2)}_{shot}\left(1+\Delta^{(2)}_{amp}\right)\right)+ \tag{20}$$
$$\Delta^{(1)}_b-\Delta^{(2)}_b$$

Under application of 17 and neglecting all $\Delta\Delta$ terms equation 20 can be simplified to:

$$\Delta I_{\mathrm{det}}(t_{IR}) \approx \frac{1}{2}\overline{I_{LO}}\cdot\left(\Delta^{(1)}_{amp}-\Delta^{(2)}_{amp}\right)+\sqrt{\frac{1}{2}\overline{I_{LO}}}\cdot\left(\Delta^{(1)}_{shot}-\Delta^{(2)}_{shot}\right) \tag{21}$$

Equation 21 shows that the resulting noise is dominated by the amplification and shot noise. These two remaining noise contributions can be separated by their different scaling with the LO intensity. We therefore measured the noise in the difference of the detector outputs as function of the LO intensity. From equation 21 we can calculate the standard deviation of the resulting deviations from the mean value yielding 22. We thereby assume equal standard deviations of the amplification noise for both channels.

$$\sigma(\Delta I_{\mathrm{det}}(t_{IR}),n) \approx \sqrt{\frac{1}{2}\left(\overline{I_{LO}}\cdot\sigma^{(1,2)}_{amp}\right)^2+\overline{I_{LO}}\cdot\left(\sigma^{(1,2)}_{shot}\right)^2} \tag{22}$$

The experiment shows a linear relation between the standard deviation of the acquired data points and the LO intensity which implies that the measured noise is dominated by the amplification noise within the range of LO intensities used in the experiment. We can therefore neglect the shot noise for this case and transform equation 22 in good approximation into 23.

$$\sigma(\Delta I_{\mathrm{det}}(t_{IR}),n) \approx \frac{\sqrt{2}}{2}\left(\overline{I_{LO}}\cdot\sigma^{(1,2)}_{amp}\right) \tag{23}$$

The sum of the detector outputs is meanwhile given by 24.

$$\Sigma I_{\mathrm{det}}(t_{IR}) = \overline{I_{LO}}\cdot\left(1+\frac{\Delta^{(1)}_{amp}+\Delta^{(2)}_{amp}}{2}\right)(1+\Delta_{\mathrm{int}})+$$
$$\sqrt{\frac{1}{2}\overline{I_{LO}}\,(1+\Delta_{\mathrm{int}})}\cdot\left[\Delta^{(1)}_{shot}\left(1+\Delta^{(1)}_{amp}\right)+\Delta^{(2)}_{shot}\left(1+\Delta^{(2)}_{amp}\right)\right]+ \tag{24}$$
$$\Delta^{(1)}_b+\Delta^{(2)}_b$$

Applying the same approximations used before 24 can be simplified to following equation:

$$\Sigma I_{\mathrm{det}}(t_{IR}) \approx \overline{I_{LO}}\,(1+\Delta_{\mathrm{int}}) \tag{25}$$

The sum of the detector outputs is consequently dominated by the intensity noise. The mean intensity of the local oscillator can be determined by simply averaging the acquired data points for the sum output (25). The desired standard deviations of the relative intensity and the amplification noise can then be determined by equations 26 and 27.

$$\sigma_{\mathrm{int}} = \frac{\sigma(\Sigma I_{\mathrm{det}}(t_r),n)}{mean(\Sigma I_{\mathrm{det}}(t_r),n)} \tag{26}$$

$$\sigma^{(1)}_{amp} = \sigma^{(2)}_{amp} = \sqrt{2}\frac{\sigma(\Delta I_{\mathrm{det}}(t_r),n)}{mean(\Sigma I_{\mathrm{det}}(t_r),n)} \tag{27}$$

The standard deviations of the noise contributions obtained for the noise measurement shown in the main text are listed below.

$$\sigma_{\mathrm{int}} = 0.1$$
$$\sigma^{(1)}_{amp} = \sigma^{(2)}_{amp} = 0.0171$$
$$\sigma^{(1)}_b = \sigma^{(2)}_b = 0.0025V$$
$$\sigma^{(1)}_{shot} = \sigma^{(2)}_{shot} \approx 0$$

5 Determination of the Components of the Measured Intensity

The mean intensity of the local oscillator can be determined from the experiment as shown in the previous section. The intensity of the SFG signal from the sample is measured using the same procedure except that in this case the infrared portion for the generation of the LO is blocked and by moving t_{IR} to maximize the signal ($\mathscr{A}(t_{IR})$=1). The amplitude of the interference term meanwhile is given by the averaged difference of the detector outputs without blocking any beams. $\mathscr{J}(t_{IR})$ can then simply be

determined using equation 28.

$$\mathscr{J}(t_{IR}) = \frac{mean(\Delta I_{het}(t_{IR}), n)}{2\sqrt{\overline{I_{LO}} \cdot \overline{I_{SFG}^{\max}}}} \tag{28}$$

For the measurement shown in the main text following values are found:

$$\overline{I_{LO}} = 1.008V$$
$$\overline{I_{SFG}^{\max}} = 0.041V$$
$$\mathscr{J}(t_{IR}) = 0.3$$

6 Calibration of the Reference Measurement

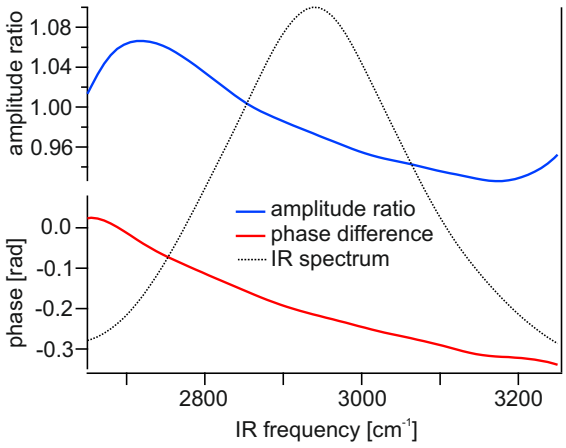

Fig. 1 Determination of the transfer-function: Amplitude (blue line) and phase (red line) of the transfer-function together with the infrared spectrum (black dotted line).

The concept of simultaneous reference sampling requires that the relative phases and amplitudes of all involved beams are equal for both the reference and the sample beam path. However, this is not necessarily the case. Each optic in the setup with polarization dependent phase change upon reflection (metallic mirrors and beam splitters) introduces slight shifts in the relative phases between LO and SFG signal (because of their orthogonal polarization). Especially a beamsplitter can additionally alter the spectrum of the pulses. All these changes are included in the spectrometer function, however, due to different beam paths of the sample and reference signals (between the oscillating mirror and the combining beamsplitter) the spectrometer functions for the sample and the reference spectrum are not exactly identical. In order to account for these differences a transfer-function is used to correct the reference spectrum. The transfer-function is determined by placing a sample (Ag mirror) such that both, sample and reference signal are generated at its surface. After data acquisition both interferograms are transferred into the frequency domain by Fouriertransformation. Assuming that the second order susceptibilities in the two spots on the sample are equal the resulting complex spectra are given by following equations (see theory section in the main text)

$$\mathscr{F}\left(I^{ref}{}_{het,bal}(t_{IR})\right) \propto \chi_{Ag}{}^{(2)}(\omega) \cdot \mathscr{S}^{ref}(\omega) \tag{29}$$

$$\mathscr{F}\left(I^{sample}{}_{het,bal}(t_{IR})\right) \propto \chi_{Ag}{}^{(2)}(\omega) \cdot \mathscr{S}^{sample}(\omega) \tag{30}$$

with the spectrometer functions $\mathscr{S}(\omega)$ and the second order susceptibility of the silver mirror $\chi_{Ag}{}^{(2)}(\omega)$. The complex transfer-function $T(\omega)$ is given by the ratio of the two complex spectrometer functions for the sample and the reference beam path.

$$T(\omega) = \frac{\mathscr{S}^{sample}(\omega)}{\mathscr{S}^{ref}(\omega)} = \frac{\mathscr{F}\left(I^{sample}{}_{het,bal}(t_{IR})\right)}{\mathscr{F}\left(I^{ref}{}_{het,bal}(t_{IR})\right)} \tag{31}$$

The resulting phase and amplitude of the transfer-function in the frequency range covered by the infrared pulses are shown in figure 1. The transfer-function reveals that the deviations between the two spectrometer functions are indeed small but in light of our aim to maximize the phase accuracy of the spectrometer it is reasonable to perform this correction. After the determination of $T(\omega)$ the reference spectra recoded in following experiments can be corrected by multiplication with this transfer-function in the frequency domain. Since the transfer-function is mainly defined by the different optics inside the reference and sample beam paths it is highly insensitive to small changes in alignment. Once determined it can therefore be used throughout entire series of experiments.

7 Calibration Translation Stage

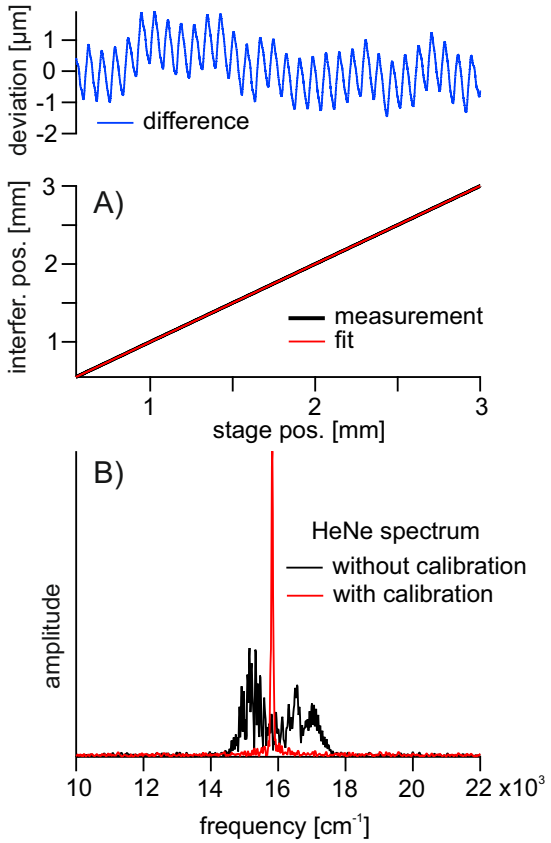

Fig. 2 Calibration of the translation state. A) Measurement of interferometric positions as function of the hardware positions (black curve) and deviation from linear fit. B) HeNe spectrum before and after calibration.

In Fourier transform spectroscopy it is essential that the data points which are sampled in the time domain are evenly spaced. To ensure this it is required that the translation stage introducing the time delays moves perfectly straight. In reality this is often not the case. For the interferometric measurements, these deviations can have drastic consequences leading to nonuniform time domain sampling which makes it in turn impossible to resolve sharp spectral features. In order to overcome this problem, the stage positions can be calibrated by recording a quadrature signal from a narrow band HeNe laser[2]. The technique is based on the interference between a circularly and a linearly polarized portion of the HeNe laser beam and allows for the accurate determination of optical distances at every stage position which can then be transformed into an interferometric stage position. The beam path inside the spectrometer for the calibration measurement is the same as for the SFG experiments to ensure a high accuracy of the calibration. The laser beam is therefore aligned along the infrared beam path and enters the interferometer (see figure 4 in the main text). The incoupling optics are replaced by transparent windows acting as beamsplitters for the visible HeNe beam. Before the two partial beams are recombined at the position of the second incoupling optic a quarter wave plate is introduced in one of the two arms generating circularly polarized light. After the recombination, there are now two HeNe beams co-propagating, one with linear the other with circular polarization. The optical path length difference between the two partial beams is meanwhile controlled by the position of the miniature translation stage which we want to calibrate. The intensity of the combined beam shows intensity modulations while scanning the translation stage caused by the interference of the two beam portions. The light then passes through the wave plate and the polarizing beamsplitter in the detection unit to be finally detected on two photodiodes. Due to the particular polarization combination (circular and linear polarization) the intensity modulations measured by the two photodiodes are phase shifted by 90 degrees. This shift is caused by mapping the circularly polarized beam portion onto two orthogonal polarization axes with the polarizing beamsplitter leading to a 90 degree phase shift between the two resulting light waves. The intensity modulations measured by the two photodiodes can therefore be described by following equations.

$$I_A = I_0 \sin(\Delta\varphi) \tag{32}$$

$$I_B = I_0 \cos(\Delta\varphi) \tag{33}$$

$$\Delta\varphi = \arctan\left(\frac{I_A}{I_B}\right) \tag{34}$$

Where I_A and I_B are the measured intensities by detector A and B after subtraction of the baseline, I_0 is the interference amplitude and $\Delta\phi$ is the phase difference between the two beam portions in the interferometer. Equation 34 shows that $\Delta\phi$ can directly be derived from the two measured intensities. This way the phase angles can be monitored for each time delay while scanning the translation stage. The obtained $\Delta\phi$ can subsequently be transformed into optical path length differences Δl using the relation

$$\Delta l = n\frac{\Delta\varphi}{2\pi}\lambda \tag{35}$$

where λ is the wavelength of the laser light and n represents the number of full phase cycles accumulated during the scan. The derived optical distances Δl can now be taken as interferometric stage positions and compared to the hardware stage positions.

The result of the calibration measurement using our spectrometer is shown in figure 2. The derived interferometric positions are plotted as a function of the hardware positions of the translation stage (figure 2A)). For a perfectly straight movement of the translation stage this function should be linear with a slope of 1. However, taking the difference between the linear fit and the measured data the discrepancy becomes evident. The apparent oscillating deviations from linearity are perfectly reproducible suggesting that their origin is a mechanical property of the translation stage. However, with this measurement in hand a calibration file can be created where each hardware position of the translation stage is correlated to a corresponding interferometric position. During a measurement, the translation stage is then set to scan over those hardware positions which correspond to the desired (equidistant) interferometric positions. The effect of this calibration can be illustrated by comparing the resulting spectra after Fourier transformation of the interferograms measured with the HeNe laser first without and then with the calibration (figure 2B)). The spectrum obtained with the calibration shows the expected narrow peak at the frequency of the HeNe laser whereas the spectrum obtained by sampling equidistant hardware stage positions can clearly not resolve the HeNe spectrum. This result demonstrates the necessity of the calibration for interferometric measurements.

8 Decomposition of Quartz Azimuthal Data

To extract the different spectral components that together compose the time domain spectra in the measured azimuthal scan we performed a singular value decomposition (SVD) of the corrected raw data matrix. The decomposition shows the presence of two spectral components which are presented in figure 5B) in the main text. In figure 5C) in the main text the azimuthal dependency of their amplitudes is shown. For better illustration of the result from the decomposition we include figure 3 which shows the separation of the measured data matrix into the sum of the two two contributing signals in their 2 dimensional representation.

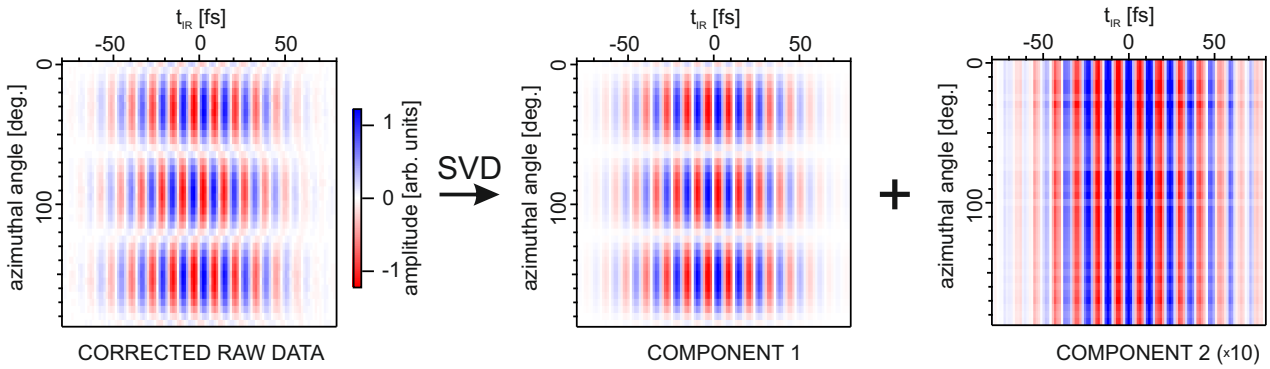

Fig. 3 Decomposition of the data matrix. left: measurement; right: azimuthal dependency of the two components.

References

1 N. Demirdöven, M. Khalil, O. Golonzka and A. Tokmakoff, *Optics Letters*, 2002, **27**, 433–435.

2 D. O. Hogenboom and C. A. DiMarzio, *Applied Optics*, 1998, **37**, 2569–2572.